Quarterly Reviews of Biophysics **42**, 4 (2009), pp. 301–316. © Cambridge University Press 2010
doi:10.1017/S003358351000028 Printed in the United States of America

Simulating activity of the bacterial ribosome

Joanna Trylska
Interdisciplinary Centre for Mathematical and Computational Modelling, University of Warsaw, Warsaw, Poland

Abstract. Computational modeling studies that investigate activity of the bacterial ribosome were reviewed. Computational approaches became possible with the availability of three-dimensional atomic resolution structures of the ribosomal subunits. However, due to the enormous size of the system, theoretical efforts to study the ribosome are few and challenging. For example, to extend the simulation timescales to biologically relevant ones, often, reduced models that require tedious parameterizations need to be applied. To that end, modeling of the ribosome focused on its internal dynamics, electrostatic properties, inhibition by antibiotics, polypeptide folding in the ribosome tunnel and assembly mechanisms driving the formation of the small ribosomal subunit.

1. Introduction 301

2. Internal motions of the ribosome 304

3. Electrostatic picture of the ribosome 306

4. Bacterial ribosome inhibition 307

5. Exploring the ribosome tunnel 309

6. Assembly of the subunits 311

7. Conclusions 313

8. Acknowledgements 313

9. References 313

1. Introduction

The ribosome is a nanoscale ribonucleoprotein complex responsible for translating genetic information in the cell from messenger RNA (mRNA) into proteins. It is composed of two subunits, which in bacteria are denoted 30S and 50S in accord with their sedimentation coefficients. The two subunits associate through a network of interactions and form the 70S active bacterial ribosome (see Fig. 1). The 50S subunit in bacteria contains more than 30 proteins that are numbered and named beginning with the letter L to indicate they are from the large subunit.

* Author for correspondence: J. Trylska, Interdisciplinary Centre for Mathematical and Computational Modelling, University of Warsaw, Zwirki i Wigury 93, 02-089 Warsaw, Poland.
Tel.: 48-22-5540-843; Fax: 48-22-5540-801; Email: joanna@icm.edu.pl

https://doi.org/10.1017/S0033583510000028 Published online by Cambridge University Press

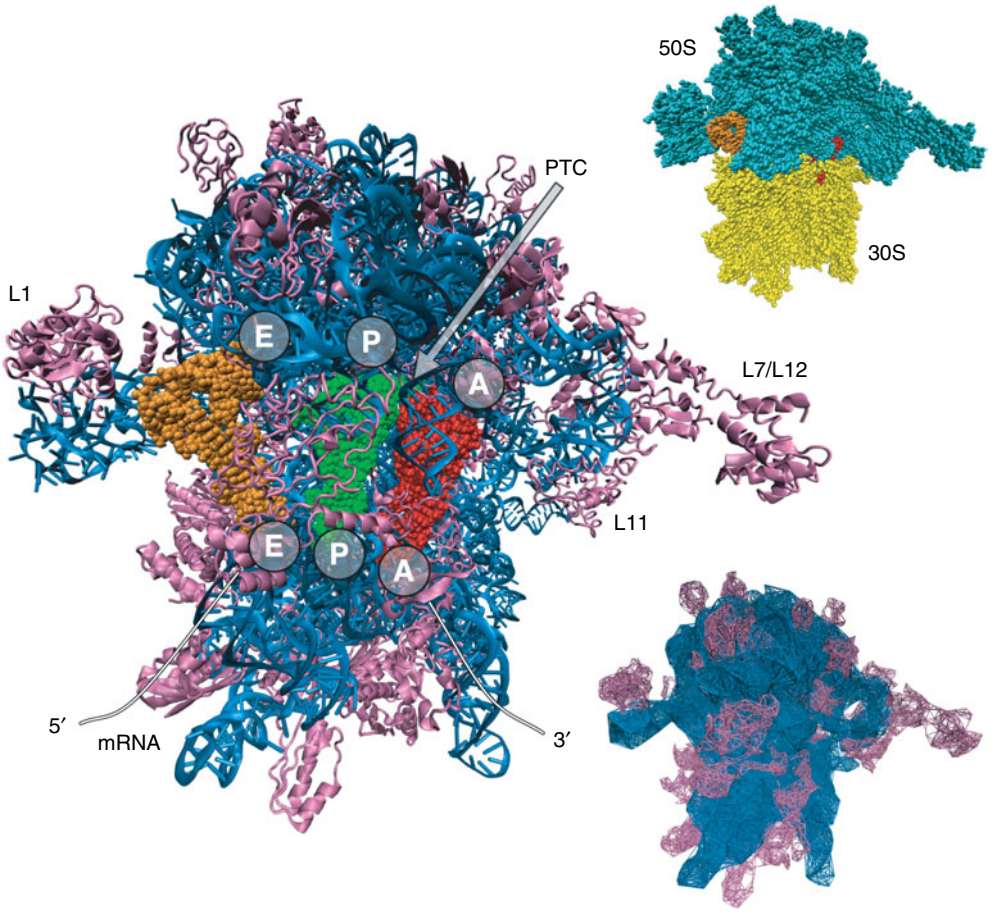


Fig. 1. 70S *Escherichia coli* ribosome cartoon model based on the 2GY9 and 2GYA PDB entries (Mitra *et al.* 2006). Ribosomal RNA is shown in blue and proteins in magenta. Three tRNA molecules shown as van der Waals spheres occupy the binding sites at the interface between subunits (A-tRNA in red, P-tRNA in green and E-tRNA in orange). Upper inset shows the division into the 30S (yellow) and 50S (cyan) subunits. Lower inset represents the ribosome as an elastic net with nodes denoting the positions of Cα carbons and P phosphorus atoms. Lines show interactions between nodes. For clarity, only Cα–Cα and P–P connections are shown.

It also contains two ribosomal RNA sequences called 23S RNA (∼2900 nucleotides) and 5S RNA (∼120 nucleotides). The 30S subunit is composed of more than 20 proteins and a single 16S RNA sequence (∼1540 nucleotides), and it binds mRNA (see Fig. 2). Proteins in the small subunit are also numbered and their names begin with the letter S.

Peptide synthesis is performed according to the nucleotide sequence of the mRNA, which is translated with the use of transfer RNAs (tRNAs) and external translation factors into the sequence of covalently bound amino acids. Amino acids are donated to the ribosome by tRNAs that bind at three sites located at interfaces between subunits: A (aminoacyl), P (peptidyl) and E (exit) (Fig. 1). The A-site accepts the incoming aminoacylated tRNA, the P-site holds the tRNA with the emerging peptide chain and the E-site holds the deacylated tRNA before it leaves the ribosome. Peptide bond synthesis occurs between the aminoacyl and peptidyl ends of A- and P-site tRNAs in the so-called peptidyl transferase center (PTC) located in the large subunit. PTC

https://doi.org/10.1017/S0033583510000028 Published online by Cambridge University Press

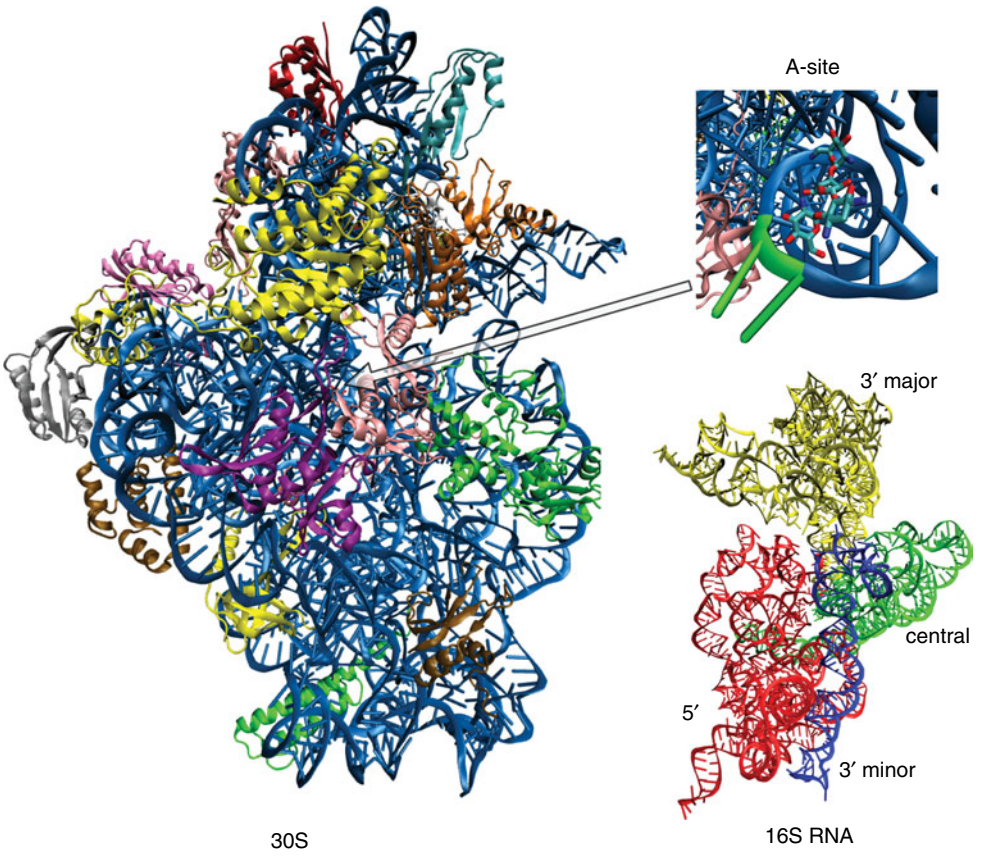


Fig. 2. Cartoon model of the 30S ribosomal subunit from *T. thermophilus* (PBD entry 1FJG) (Carter *et al.* 2000). 16S RNA is in blue. Upper inset shows paromomycin bound in the A-site with two adenines A1492 and A1493 (green) in a flipped-out state. Lower inset shows the domains of 16S RNA with 5′ domain in red, central in green, 3′ major in yellow and 3′ minor in dark blue.

is formed of RNA, making the ribosome a ribozyme; for a review of the mechanism of peptide bond formation on the ribosome, see Rodnina *et al.* (2006). After the reaction, tRNAs co-operatively translocate to their new positions (P and E) with the advance of mRNA by exactly one codon. The E-site tRNA is then ready to leave the ribosome and a new tRNA may bind in the A-site. The nascent polypeptide leaves the ribosome through a 10-nm-long and about 2-nm-wide tunnel located inside the 50S subunit.

Translation is a complex and multistep process (Liljas, 2004; Wilson & Nierhaus, 2003). The events occurring in four principal stages of bacterial translation (initiation, elongation, termination and recycling) are modulated by various external factors binding to the ribosome. The key factors of translation in bacteria include initiation factors, IF-1, IF-2 and IF-3, which assist in subunit association. Elongation factors Tu (EF-Tu) and G (EF-G) facilitate the elongation stage. EF-Tu-GTP complexes with the aminoacyl-tRNA and in the form of ternary complex associates with the ribosome and delivers tRNA to the A-site. When the appropriate charged tRNA is deposited into the A-site, the GTP is hydrolyzed, the A-tRNA is accommodated and the EF-Tu-GDP is released. Next, EF-G associates and at the expense of GTP promotes the translocation of tRNAs and mRNA. Later, when a stop codon is encountered, the release factors (RF-1, RF-2

https://doi.org/10.1017/S0033583510000028 Published online by Cambridge University Press

and RF-3) control the termination stage. Ribosome recycling factor (RRF) facilitates subunit dissociation and release of mRNA. Therefore, precise binding of all these factors must occur in exactly the correct phase of translation.

Peptide synthesis in bacteria is inhibited by many antibiotics that bind to specific sites (mainly RNA) on the ribosome (Hermann, 2005; Liljas, 2004; Poehlsgaard & Douthwaite, 2005). Some antibiotics prevent the association or dissociation of translation factors, while others hinder the incorporation of tRNAs, inhibit functional conformational changes of the ribosome or prevent the nascent peptide from leaving the ribosome. For example, aminoglycosidic antibiotics bind to the 16S RNA in the 30S subunit and interfere either with decoding or translocation of tRNAs. Other exemplary classes of antibiotics are macrolides that bind to the 23S RNA of the 50S subunit in the proximity of the PTC and restrict the egress of the polypeptide from the ribosome exit tunnel. Bacteria constantly develop resistance against various antibiotic classes; therefore, extensive research is devoted to aspects of antibiotic–ribosome binding in order to help seek novel antibacterial agents.

Structural studies of the ribosome have been carried out for many decades and at the turn of the millennium resulted in structures on atomic resolution. With the appearance of the all-atom crystal structures of the 30S (Schluenzen *et al.* 2000; Wimberly *et al.* 2000), 50S subunits (Ban *et al.* 2000; Harms *et al.* 2001) and subsequently of a 5·5-Å resolution structure of the entire 70S ribosome (Yusupov *et al.* 2001), computational modeling of the ribosome on a nearly atomic scale became possible. These structural data once deposited into the Protein Data Bank (Bernstein *et al.* 1977) provided great opportunities to examine functional, dynamic and electrostatic properties of the prokaryotic ribosome using various simulation techniques. Nevertheless, from the point of view of theoretical methods, modeling the entire ribosome or its subunits even though feasible is still challenging due to system size. The 30S subunit is composed of approximately 90 000 atoms with dimensions of about $21 \times 18 \times 20$ nm^3. The 50S subunit is even larger and consists of nearly 150 000 atoms. Altogether, the number of atomic nuclei in bacterial ribosome exceeds 240 000 (excluding the surrounding first-solvation shell water molecules or counter-ions), with overall dimensions of 25 nm^3.

Simulations of the ribosome can help researchers understand, explain and analyze experimental biochemical data. However, there are cases where the simulations have predictive power as well. I review computational efforts to investigate the functioning of entire bacterial ribosome or its subunits focusing on the studies based on structural data that appeared in the beginning of this century.

2. Internal motions of the ribosome

Structural experiments of cryo-electron microscopy (cryo-EM) (Frank, 2003), X-ray crystallography (Bashan & Yonath, 2008) and fluorescence resonance energy transfer (FRET) (Munro *et al.* 2008) have shown that the ribosome is a dynamic machine and its various parts are involved in functional motions. For a recent review of experimental observations of the 'moving' ribosome, see Korostelev *et al.* (2008). For example, a ratchet-like motion of the subunits related to translocation of tRNAs and mRNA was initially found by cryo-EM studies (Frank & Agrawal, 2000; Gabashvili *et al.* 1999). Later, it was also postulated that translocation involves a significant movement of the L1 stalk (Fig. 1), which helps the E-site tRNA to leave the ribosome (Valle *et al.* 2003). The opposite L7/L12 stalk belonging to the 50S subunit also undergoes extensive motions and together with L10 and L11 proteins helps accommodate elongation factors.

https://doi.org/10.1017/S0033583510000028 Published online by Cambridge University Press

Elongation factors themselves were also found to undergo large structural rearrangements upon binding to the ribosome (Liljas, 2004). Structural dynamics of the ribosome observed by combining and comparing different cryo-EM and X-ray crystallography models was supplemented and extended by computational modeling. Several theoretical investigations examined the internal motions of the ribosome both on a coarse-grained and an all-atomic scale. Two powerful computational techniques to study the dynamics, normal mode analysis (NMA) and molecular dynamics (MD) were applied (Schlick, 2002). In NMA, a system's motions are decomposed into independent vibrational modes (directions in configurational space) characterizing fluctuations from an equilibrium structure. This is achieved by diagonalizing the matrix of the second derivatives of the potential energy. In MD, the positions and velocities of individual particles in the system as a function of time are generated by integrating Newton's laws of motion.

Chacon *et al.* (2003) explored ribosome internal motions by representing the ribosome as elastic net with interactions modeled as harmonic springs. Their model was based on the 25-Å cryo-EM density map. Next, the authors applied NMA, derived the lowest-frequency vibrational modes of the ribosome and observed the ratchet-like motion of the 30S subunit relative to the 50S subunit. This suggested that the rotational movement is an inherent property resulting from the shape of the ribosome that can as a first approximation be treated as an elastic body. Global motions often correspond to functional motions and do not depend on the details of the potential energy function. This observation was in accord with biochemical experiments that had shown that peptide synthesis on the ribosome could occur (with greatly reduced efficiency) without the expense of GTP and translation factors (Gavrilova *et al.* 1976; Southworth *et al.* 2002).

A more detailed study applied NMA to explore the internal dynamics of the ribosome based on the 5·5-Å resolution crystal structure (Tama *et al.* 2003; Wang *et al.* 2004). In this model, the crystallographically determined positions of phosphate and Cα carbon nuclei served to build the elastic net of the ribosome (Fig. 1) and subsequently to calculate the lowest frequency modes. These low-energy modes showed the ratchet-like relative motion of the subunits. Moreover, displacement of the L1 ribosomal stalk that serves to open and close the intersubunit space near the E-site was observed. The L11 protuberance on the other side of the ribosome also exhibited a large-scale motion. These studies approximated the fluctuations as harmonic and isotropic but a more recent normal mode study of the ribosome dynamics accounted also for anisotropic fluctuations (Kurkcuoglu *et al.* 2008). The authors found that the removal of L1 and L7/L12 stalks preserves the rotational movement of the subunits as well as the rotation of the head of the 30S subunit.

In NMA, the motions can only be characterized separately one at a time. Therefore, to overcome this drawback and to increase the level of detail of the dynamics, a reduced MD simulation of the ribosome was performed, which also accounted for some anharmonicity of motions (Trylska *et al.* 2005b). The extension of the elastic network model (Fig. 1) included all-atom like potential energy functions that distinguished both local bonded and non-local non-bonded interactions. The parameterization was based on pair distribution functions derived from the low-resolution crystal structure of the ribosome (Yusupov *et al.* 2001). Half a microsecond MD simulation timescales were achieved. This study found that the movements of L7/L12 and L1 lateral stalks are anti-correlated and span a range up to 15 Å. Ratchet-like rotation of the subunits correlated with the movement of the L1 stalk was also observed. The 50S subunit was found to undergo many local internal fluctuations and the 30S subunit was more compact and moving as one uniform block. The tRNA CCA-3′ termini and anticodons exhibited small

https://doi.org/10.1017/S0033583510000028 Published online by Cambridge University Press

fluctuations which suggested tight alignment of substrates during the formation of peptide bond and decoding.

The above presented reduced modeling of the internal dynamics of the ribosome has proven that the ribosome internal mobility arises due to its shape and is inherent to the system. The most important slowest motions are robust and not sensitive to the details of the structure and even low-resolution structural data are enough to determine global collective dynamics. Global functional motions and rearrangements are, therefore only accelerated by GTP. It was found that translation is possible without GTP hydrolysis and can indeed be factor-free (Gavrilova *et al.* 1976; Southworth *et al.* 2002) so the studies were in accord with experimental data.

In 2005 Sanbonmatsu and coworkers (Sanbonmatsu *et al.* 2005) published the first all-atom MD simulation of the entire ribosome in explicit solvent. The study focused on the mechanisms leading to proper incorporation of tRNA into the ribosomal A-site. The all-atom homology model of the *T. thermophilus* 70S ribosome was used as the initial configuration (Tung & Sanbonmatsu, 2004) and the resulting simulation box consisted of 2·64 million atoms. MD were performed on the Los Alamos National Laboratory ASCI Q-machine supercomputer using 512, 768 and 1024 processors and about 106 computer hours. The overall timescale of the simulation was about 20 ns. The authors simulated the accommodation of aminoacyl-tRNA with many targeted MD 2-ns-long runs by gradually reducing the root mean square deviation of the starting structure toward the final A-tRNA configuration. Recently, all-atom MD simulations of the 30S ribosomal subunit involving 1·07 million atoms were also performed (Sanbonmatsu & Tung, 2007).

3. Electrostatic picture of the ribosome

Electrostatics, due to its long-range nature, plays a pivotal role in many biological processes. Biomolecules are characterized by complicated charge distributions and electrostatic forces often dominate their intermolecular and intramolecular interactions. Therefore, a proper description of the electrostatic potential around molecules is an important aspect of computational approaches. The most common and successful method used to obtain electrostatic properties of biomolecules is the Poisson–Boltzmann model (Baker, 2004; Honig & Nicholls, 1995). A molecule described by a set of fixed partial charges and radii is immersed in implicit solvent with ionic strength. The molecule is assigned a low dielectric constant, in the range of 4 to 12, and the solvent is assigned a high dielectric constant of 80, corresponding to water. The local ionic concentrations are described by the Boltzmann distribution. To obtain the electrostatic potential, the so-called Poisson–Boltzmann equation is solved with numerical techniques on a three dimensional grid covering the molecule and its surroundings. The distance between the grid points defines the resolution of the calculation.

First efforts to determine the electrostatic potential around entire ribosome subunits arose due to the development of the Adaptive Poisson–Boltzmann Solver (Baker *et al.* 2001). The software was designed to solve the Poisson–Boltzmann equation for large nanoscale systems. The authors calculated the electrostatic properties of all-atomic structures of the small and large ribosomal subunits. Calculations used 343 processors of the NPACI Blue Horizon supercomputer at the San Diego Supercomputer Center and were performed with a grid resolution of 0·4 Å. The calculated electrostatic potential around the subunits was mainly negative due to the presence of negatively charged phosphate groups of RNA. Positive potential areas resulted from the ribosomal proteins and the presence of counter-ions. There was a qualitative electrostatic

https://doi.org/10.1017/S0033583510000028 Published online by Cambridge University Press

complementarity of the 50S and 30S subunit potential surfaces at interfaces that associate to form the ribosome. The authors found that the codon-binding sites are surrounded by positive potential regions that could aid the stabilization of tRNAs and mRNA. The proteins of the large subunit involved in tRNA binding also exhibit positive potential patches.

It was shown that during translation, the ribosome undergoes large-scale conformational changes that are relevant to its function (Frank & Agrawal, 2000; Gabashvili *et al.* 1999). One of these changes is the ratchet-like rotation of the subunits that takes place in the polypeptide elongation phase. We explored the changes in the electrostatic potential around the ribosome during this ratchet-like motion of the subunits (Trylska *et al.* 2004). The conformations of the ratcheting motion were derived from the NMA (see Section Internal dynamics of the ribosome) based on the 5·5-Å resolution crystal structure of the entire bacterial ribosome (Yusupov *et al.* 2001). At that time, only a low-resolution structure of the 70S ribosome was available providing the positions of Cα and P atomic nuclei. Thus, to study electrostatic properties of the ribosome, a reduced electrostatics Poisson–Boltzmann model was developed. We found that the electrostatic potential around the ribosome is mainly negative due to the fact that two-thirds of the ribosomal mass arises from the RNA. This was in accord with the previous electrostatic study (Baker *et al.* 2001) on the individual subunits. However, positive patches of the electrostatic potential are present and come mainly from the positively charged proteins. Positive electrostatic potential was observed in the areas where the EF-G, EF-Tu and release factors bind. Changes in the electrostatic potential along the ratchet-like displacement were seen mainly in the tRNA binding sites. This study also showed the complementarity of the long-range electrostatic potential between EF-G and its binding site. The L1 protein was found to be a source of positive potential possibly facilitating the release of E-site tRNA from the ribosome. The PTC, being bare of proteins, is characterized by a negative electrostatic potential. Large positive-potential spots are associated mainly with proteins L6, L11, S12 and S19.

Nowadays, all-atomic Poisson–Boltzmann calculations of the electrostatic potential around the ribosome are possible. Figure 3 presents the electrostatic potential projected on the molecular surface of the entire 70S ribosome. The all-atom derived electrostatic potential confirms the earlier potential maps derived for the reduced ribosome model. Many strongly negative patches are observed even though neutral and positive areas corresponding mainly to proteins do appear.

4. Bacterial ribosome inhibition

Blocking the bacterial ribosome function leads to inhibition of microbial growth, which is important in alleviating bacterial infections. Antibiotics targeting the ribosome bind to both the 50S and the 30S subunit (Poehlsgaard & Douthwaite, 2005). The first antibiotics for which the crystal structure in the complex with the 30S subunit was solved were aminoglycosides (Carter *et al.* 2000); therefore, computational studies of antibiotic association and binding to the ribosome were initially performed for this class of compounds.

Aminoglycosides, such as paromomycin and neamine, are positively charged sugar derivatives that bind in the A-site of the 30S subunit and interfere with the decoding (see Fig. 2). They lock the two decoding bases in their extra-helical state, which makes the ribosome accept non-cognate tRNAs and incorporate incorrect amino acids into the nascent peptide. The first theoretical study to determine the energetics of binding of aminoglycosides to the entire 30S subunit was performed by Ma *et al.* (2002). Based on the continuum solvation Poisson–Boltzmann model

https://doi.org/10.1017/S0033583510000028 Published online by Cambridge University Press

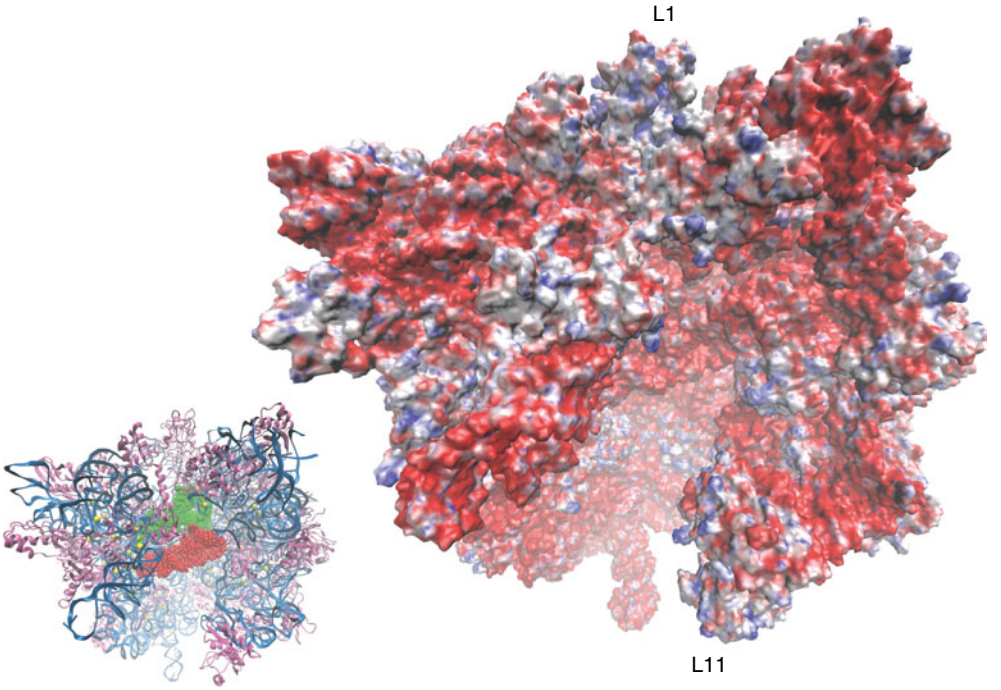


Fig. 3. The electrostatic potential of the all-atom *E. coli* 70S ribosome in the pre-translocational state (3DF3 and 3DF4 PDB entries) (Borovinskaya *et al.* 2008) mapped onto its molecular surface. The Poisson–Boltzmann calculations were conducted at monovalent ionic strength of 150 mM. Color scale changes from red $\leqslant -5$ kT/e, through white 0 kT/e to blue $\geqslant +5$ kT/e. The inset shows the positions of A-tRNA (in red) and P-tRNA (in green). Ribosomal RNA is shown in blue and proteins in magenta. Magnesium ions present in the crystal structure are represented as yellow van der Waals spheres. L7/L12 stalk was not resolved in this structure.

combined with the surface area-dependent nonpolar term, the authors calculated the binding free energies for a set of aminoglycosides. Good agreement with experimental data was obtained, showing promise for further studies. Later, Yang *et al.* (2006) extended the previous model by additionally estimating the entropy loss of aminoglycosidic rings upon binding, as well as the translational and rotational entropy changes. The parameters of the model for the 30S subunit were determined based on calculations and experimental studies performed for a smaller A-site oligonucleotide. These studies have shown that despite many approximations, the implicit solvent Poisson–Boltzmann model can reproduce the overall binding hierarchy of antibiotics to the 30S subunit. The models were able to perceive small charge perturbations caused by different functional groups in the antibiotic rings.

Studies that focused on the diffusion of aminoglycosides toward the 30S subunit were also performed. By means of Brownian dynamics, we have recently investigated the rates of association of paromomycin to the whole 30S subunit (Dlugosz & Trylska, 2009). We found that the antibiotic first diffuses toward the subunit and then explores its surface to encounter the A-site. During the pathway leading to binding in the A-site, paromomycin also interacts with other cavities that are the binding sites for other antibiotics. In general, the mobility of paromomycin in the A-site was found to be high and the antibiotic could enter the A-site from two opposite sides.

https://doi.org/10.1017/S0033583510000028 Published online by Cambridge University Press

Another recent study (Aleksandrov & Simonson, 2008) focused on tetracycline – another known antibiotic targeting the 30S subunit. Molecular dynamics (including 30S subunit atoms within 26 Å around the antibiotic) combined with Poisson–Boltzmann continuum electrostatics was applied to determine tetracycline binding free energies to two crystallographically determined binding sites in the 30S subunit. In accord with experimental electron density maps, the authors confirmed the existence of tetracycline primary binding site, suggesting that other sites are weaker and less occupied.

The mechanism of gentamicin binding to the A-site was investigated by replica-exchange MD simulations of the ribosomal decoding site (Vaiana & Sanbonmatsu, 2009). The two decoding bases were found to flip in and out of the A-site RNA on a timescale faster than antibiotic binding suggesting a stochastic gating mechanism where the ligand does not induce flipping out of the bases but only traps them in a flipped out state. Gentamicin was found to explore various minima in its binding site. The movement of these two decoding bases A1492 and A1493 was also previously studied on the fragments of the ribosomal RNA with and without the antibiotic (Meroueh & Mobashery, 2007; Reblova *et al.* 2006; Romanowska *et al.* 2008; Sanbonmatsu, 2006).

Ribotoxins are another class of ligands that recognize the ribosome and compete with the binding of elongation factors. They bind with a high association rate constant exceeding $10^{10}\ \mathrm{M}^{-1}\ \mathrm{s}^{-1}$ at low ionic strengths. Ribotoxins cleave a specific nucleotide of 50S subunit ribosomal RNA, which hinders the binding of elongation factors, leading to disruption of protein synthesis. Calculations of binding rate constant of restrictocin belonging to ribotoxin family were recently performed giving physical insight into the reasons for its high value (Qin & Zhou, 2009).

5. Exploring the ribosome tunnel

Before the release from the ribosome into the crowded cellular environment, the newly synthesized polypeptide travels through a 100-Å-long tunnel located inside the 50S subunit. The diameter of the tunnel varies between 10 and 20 Å and its walls are made mainly of ribosomal RNA. Three distinct areas of the tunnel can be identified: the entrance, the constriction and the exit, which is the widest part (Jenni & Ban, 2003). Two extensions of proteins L22 and L4 protrude inside the tunnel in its narrowest part and are believed to function as a discriminating gate for certain polypeptide sequences (Nakatogawa & Ito, 2002; Tenson & Ehrenberg, 2002). Several antibiotics, such as erythromycin, bind close to the entrance of the tunnel and block the path of the emerging polypeptide. The tunnel itself is believed to provide a constrained environment for co-translational folding, especially in case of α-helices. An exemplary biochemical study (Lu & Deutsch, 2005) found that helices form inside the ribosome at certain tunnel locations. The helix formation depends on the polypeptide sequence (resulting in a particular helix propensity), the length of the nascent chain and which zone of the tunnel it occupies. Geometric analysis of the tunnel (Voss *et al.* 2006) based on the structure of large ribosomal subunit showed that there are regions where water molecules and ions can freely diffuse in and out of the tunnel not only through its exit but also through other passages. The interior of the large ribosomal subunit is therefore permeable to water molecules.

Computational modeling studies of the ribosome tunnel were performed to resolve both its mechanistic properties and the nature of folding and translocation of polypeptides in such a constrained environment. Coarse-grained methods were mostly applied. Coarse-grained

https://doi.org/10.1017/S0033583510000028 Published online by Cambridge University Press

Langevin dynamics simulations of polypeptide folding in the cylindrical tunnel, mimicking that of the ribosome, confirmed that confinement could entropically stabilize α-helices (Ziv *et al.* 2005). Residues were represented based on the positions of Cα carbons and were divided into two classes: hydrophilic and hydrophobic. The potential energy function was a sum of analytical terms and a confining potential with a cylindrical symmetry was used. The peptides of the length between 9 and 47 amino acids were studied, and the authors found that inside the model tunnel longer helices were more stabilized than short ones. Helix stabilization may be due to the fact that the diameter of the ribosome tunnel is close to that of an α-helix.

Translocation of the β-hairpin-forming peptide through a tunnel that mimics the one in the ribosome was also studied (Kirmizialtin *et al.* 2004). The peptide consisted of Cα carbons connected by virtual 3·8-Å-long bonds. The peptide residues were divided into three classes: hydrophobic, hydrophilic and neutral. The potential energy function was presented as a sum of bonded and nonbonded analytical terms in a similar manner as in all-atom force fields. The movement of the polypeptide via a cylindrical tunnel of various diameters was modeled with Langevin dynamics. The authors found that when the diameter of the tunnel decreases below a critical value of about 13·7 Å, the peptide assumes an extended configuration. In a wider tunnel, the peptide is stabilized in the folded state regardless of its location inside the tunnel. As the peptide progresses toward the tunnel exit, its free energy decreases.

On the other hand, Elcock (2006), who studied the path of a polypeptide through the ribosome tunnel with a Go-like folding model (Go, 1983), found that confinement of the emerging polypeptide does not necessarily promote formations of the native structure during synthesis. Three model proteins were studied: chymotrypsin inhibitor 2, barnase and Semliki forest virus protein. Amino acids were gradually added at the ribosome PTC, and their movement through the large subunit tunnel was generated according to Brownian dynamics protocol. The large subunit was represented at a near-atomic level and the nascent proteins with Cα carbons only. Standard molecular mechanics terms were used to model bonded interactions in proteins. The nonbonded interactions for residues that are in proximity (direct contact) in the folded state were assumed attractive and all others repulsive. Brownian dynamics simulations suggested that simple confinement of the protein within the tunnel did not significantly affect its folding.

Mechanistic properties of the ribosome tunnel were studied with a coarse-grained anisotropic elastic network model combined with NMA (Kurkcuoglu *et al.* 2009). The simulations confirmed the existence of three distinct regions of the tunnel characterized by different motions. The entrance region, beginning at the PTC, shows motions propagating in the direction of the exit of the tunnel. The narrow part of the tunnel (i.e. the neck or constriction) shows a rotational motion. The exit region is characterized by highest amplitude motions in a direction perpendicular to the exit path. A coarse-grained polypeptide chain in an extended conformation was inserted inside the tunnel but its presence did not affect the overall dynamics of the tunnel.

Molecular dynamics technique was used to study the path of the 36-residue polyalanine inside the ribosome tunnel (Ishida & Hayward, 2008). The system composed of 1·9 million atoms including the 70S ribosome, explicit solvent and counter-ions was simulated for a total time of 20 ns. The results showed that the extended loops of L4 and L22 proteins partially close the tunnel and hinder the passage of the polyalanine. Additionally, the polyalanine peptide was pulled through this constriction with steered MD. The authors claim that the progressing polypeptide changes the conformation of Arg92 of L22 from a position closing the tunnel to an open one. Arg92 acts as a conformational switch that opens the gate for the polypeptide. The global motions of the tunnel were not observed in such a short timescale of the simulations, and it was

https://doi.org/10.1017/S0033583510000028 Published online by Cambridge University Press

proposed that the tunnel does not act as a peristaltic pump, but the peptide moves due to its own flexibility and/or the decrease of the electrostatic potential inside the tunnel.

Still, more studies are needed to determine the influence of the ribosome tunnel on the folding of synthesized polypeptides.

6. Assembly of the subunits

The assembly of the ribosome and its subunits is a complicated process that can spontaneously occur under certain conditions, also *in vitro*. This means that all the information required for the proper ribosome assembly is present only in the ribosomal RNA and protein components. The assembly of the 30S subunit was found to be a sequential and cooperative process. The first experimental small subunit assembly map was determined by Held *et al.* (1974). It classified the proteins into three groups: primary binders that could bind to the bare 16S RNA, secondary binders that could bind only after one of the primary proteins was bound and tertiary proteins that could bind only after at least one primary and at least one secondary protein was bound. In 1993, Powers *et al.* (1993) performed chemical foot-printing studies and resolved a kinetics-based 30S assembly map. They classified proteins into early, middle, middle-late and late binders and suggested that assembly proceeds mostly from the 5′ to the 3′ end of 16S RNA. The most recent study by Talkington *et al.* (2005) of the 30S subunit kinetics assembly landscape determined the association rate constants for individual 30S proteins using mass spectrometry. A review of the 30S subunit assembly biophysical studies is provided by Williamson (2008).

The 16S RNA can be divided into three main domains presented in Fig. 2: 5′, central, and 3′ (further divided into 3′ major and 3′ minor). The crystal structures have shown that majority of the 30S proteins interact exclusively with individual 16S RNA domains. The above experimental studies indicated a few pathways in the assembly process corresponding to the 16S RNA domains and together with the 30S subunit crystal structures paved the way to computational modeling studies of the assembly process.

Stagg *et al.* (2003) explored the 3′ domain assembly path using the coarse-grained Monte Carlo simulated annealing technique. The one-bead per nucleotide and amino acid model was applied with harmonic interactions for pseudo-bonds, pseudo-angles and pseudo-torsions and a volume exclusion term disallowing the overlap of beads (Malhotra *et al.* 1994). Specific protein-RNA interactions were represented with Morse-like potential which served as a restraint to guide certain proteins to their appropriate binding sites. Additional pseudo-atoms were added between RNA strands that formed helical structures to maintain their overall fold. The 16S RNA starting model contained information only on its secondary structure. The 30S proteins were sequentially added to the 16S RNA starting from a random position. The authors examined the changes in fluctuations of 16S RNA upon binding of proteins to the 3′ RNA domain (S7) path. This way they could predict the contributions of each protein to the organization of their binding sites. Their results suggested that the binding sites for primary binders were more ordered in the bare 16S RNA than the sites for other proteins. Therefore, binding of primary proteins reduces the flexibility of 16S RNA and the primary binders also tend to organize the binding sites on RNA for later binding proteins.

Another theoretical modeling of the 30S assembly map was based on the Poisson–Boltzmann model and calculations of the energetics of binding (Trylska *et al.* 2005a). We investigated the relative binding free energies of various 30S proteins to the 16S RNA to determine the most probable assembly path based on the energetics of binding. The electrostatic, nonpolar and

https://doi.org/10.1017/S0033583510000028 Published online by Cambridge University Press

entropic contributions to binding were taken into account. The Poisson–Boltzmann electrostatic energies were calculated on 300 processors of NPACI Data Star and 800 processors of Blue Horizon Supercomputers up to 0·2-Å grid resolution. Results demonstrated that for the majority of proteins electrostatics opposes binding, even though all except one of the 30S proteins carries a positive net charge. This means that it is more favorable for proteins to interact with the high dielectric solvent than with the ribosomal RNA. Overall, the 5′ RNA domain proteins that bear the highest positive charge, get buried the most upon binding to 16SRNA and are the strongest binders. A computationally derived binding affinity map was constructed, which classified the proteins according to the strength of interactions with the 16S RNA and 30S subunit. Even though the map was only qualitative and based on relative binding free energies, it proved the ability of the computational models to be applied not only to single proteins and small ligands but also to macromolecular assemblies composed of proteins and RNA.

To study the flexibility of 16S RNA during binding of 30S proteins, (Cui *et al*. 2006) employed a similar model as Stagg *et al*. (2003), but to assess the system's fluctuations, they used MD. They performed multiple 100-ns-long Langevin dynamics simulations and analyzed the conformational changes of 16S RNA in the bound and unbound forms. The authors studied mainly the 3′ RNA domain (i.e. the S7) assembly path and found structural explanations for the sequential binding of proteins in this path. In particular, they found that the presence of primary and secondary proteins (S7 and S9) helps to organize the binding sites for tertiary proteins. Primary proteins help in stabilizing 16S RNA, whose configuration, while bare of proteins, deviates significantly from the crystal structure and acquires an extended-like form. If a tertiary protein is allowed to bind first, then the root mean square deviation of 16S RNA is similar to the one in its unbound form. In the protein-bound 16S RNA, the central domain is the most stable and the 3′ minor domain is the least stable.

The dependence of proteins on each other's binding to 16S RNA was also studied with another reduced model (Hamacher *et al*. 2006). Each nucleotide and amino acid was represented as a single interacting center. The binding free energy was approximated by harmonic interactions along the backbones and within a certain cutoff distance. Bead-specific contact energy was also applied and the Hamiltonian of the system was integrated by an analytical method. The approach focused on changes in both energetics and fluctuations. The interdependencies of protein binding were deduced by removing one or two proteins at a time from the full 30S complex. The binding free energies were computed as the difference between the energy of the complex and binding partners. The key proteins contributing to mutual stabilization were identified and the stabilizing effect of each protein on the remaining ones was quantified. These influences were found to be caused by nonlocal effects. For example, proteins S15, S16 and S20 were found not to influence binding of other proteins.

Recently, a similar dependence-based study was conducted (Yan *et al*. 2008) but was based on the dynamical effects derived from NMA. The 30S system was represented as an elastic network formed by Cα and P atoms connected by harmonic springs. The motions were analyzed based on anisotropic network model that takes into account the directionality of fluctuations and their anisotropy. The authors removed single proteins, pairs of proteins and various sets of proteins from the 30S complex and studied the effect of this removal on internal mobility of the remaining part of the 30S subunit. It turned out that the motions of the 16S RNA alone and inside the complete 30S subunit are very close. This means that the motion of the bare 16SRNA is determined by its shape alone and that the intermolecular interactions between 16S RNA and the 30S proteins do not affect the dynamics of 16S RNA in the complex. The normal modes

https://doi.org/10.1017/S0033583510000028 Published online by Cambridge University Press

dynamics also predicted that proteins S6 and S18 behave as one block, which is in accord with previous studies showing that these two proteins bind as a dimer (Hamacher *et al.* 2006; Held *et al.* 1974; Powers *et al.* 1993).

To date, no similar studies on the 50S subunit were performed. The reason is that the number of proteins in the 50S subunit is larger than in the 30S subunit and at least over 30 proteins would need to be classified. Moreover, the overall net charge of the large subunit is around −3000e, which makes this subunit a more difficult system to study with the known electrostatic models. The experimental approaches to the 50S subunit assembly are reviewed by Klein *et al.* (2004).

7. Conclusions

Thanks to high-resolution structural data of the bacterial ribosome, various modeling approaches gave more insight into its function and dynamics. Studies of ribosome internal dynamics analyzed both the collective motions and the details of the decoding process. Electrostatic calculations characterized the electrostatic picture of the ribosome. Various binding free energy techniques helped assess the energetics and kinetics of binding of antibiotics to the 30S subunit. Modeling of the 30S proteins' assembly paths gave insight into what drives the formation of the small ribosomal subunit. Despite the large size and high complexity of the ribosomal machine, all the molecular modeling efforts in the last years were proven to be useful, corroborated and extended experimental data. However, modeling tools to be applicable to such nanoscale systems still need development. In the future, computational modeling should definitely focus not only on the prokaryotic but also on the more complex eukaryotic ribosomes once structural data of better resolution on the eukaryotic 80S ribosome become available.

8. Acknowledgements

The author acknowledges support from University of Warsaw (ICM BST 2008, BST 2009, G31-4), Polish Ministry of Science and Higher Education (N N301 245236), Fogarty International Center (NIH grant R03 TW07318) and Foundation for Polish Science (Focus program and Team project co-financed by European Regional Development Fund operated within Innovative Economy Operational Programme). Figures were prepared under visual molecular dynamics (Humphrey *et al.* 1996).

9. References

Aleksandrov, A. & Simonson, T. (2008). Molecular dynamics simulations of the 30S ribosomal subunit reveal a preferred tetracycline binding site. *Journal of the American Chemical Society* **130**, 1114–1115.

Baker, N. A. (2004). Poisson–Boltzmann methods for biomolecular electrostatics. *Numerical Computer Methods, Pt D* **383**, 94–118.

Baker, N. A., Sept, D., Joseph, S., Holst, M. J. & McCammon, J. A. (2001). Electrostatics of nanosystems: application to microtubules and the ribosome. *Proceedings of the National Academy of Sciences USA* **98**, 10037–10041.

Ban, N., Nissen, P., Hansen, J., Moore, P. B. & Steitz, T. A. (2000). The complete atomic structure of the large ribosomal subunit at 2·4 angstrom resolution. *Science* **289**, 905–920.

Bashan, A. & Yonath, A. (2008). Correlating ribosome function with high-resolution structures. *Trends in Microbiology* **16**, 326–335.

Bernstein, F. C., Koetzle, T. F., Williams, G. J. B., Meyer, E. F., Brice, M. D., Rodgers, J. R., Kennard, O., Shimanouchi, T. & Tasumi, M. (1977). Protein Data Bank – Computer-based archival file for

https://doi.org/10.1017/S0033583510000028 Published online by Cambridge University Press

macromolecular structures. *Journal of Molecular Biology* **112**, 535–542.

Borovinskaya, M. A., Shoji, S., Fredrick, K. & Cate, J. H. D. (2008). Structural basis for hygromycin B inhibition of protein biosynthesis. *RNA* **14**, 1590–1599.

Carter, A. P., Clemons, W. M., Brodersen, D. E., Morgan-Warren, R. J., Wimberly, B. T. & Ramakrishnan, V. (2000). Functional insights from the structure of the 30S ribosomal subunit and its interactions with antibiotics. *Nature* **407**, 340–348.

Chacon, P., Tama, F. & Wriggers, W. (2003). Mega-Dalton biomolecular motion captured from electron microscopy reconstructions. *Journal of Molecular Biology* **326**, 485–492.

Dlugosz, M. & Trylska, J. (2009). Aminoglycoside association pathways with the 30S ribosomal subunit. *Journal of Physical Chemistry B* **113**, 7322–7330.

Elcock, A. H. (2006). Molecular Simulations of cotranslational protein folding: fragment stabilities, folding cooperativity, and trapping in the ribosome. *Plos Computational Biology* **2**, 824–841.

Frank, J. (2003). Electron microscopy of functional ribosome complexes. *Biopolymers* **68**, 223–233.

Frank, J. & Agrawal, R. K. (2000). A ratchet-like inter-subunit reorganization of the ribosome during translocation. *Nature* **406**, 318–322.

Gabashvili, I. S., Agrawal, R. K., Grassucci, R., Squires, C. L., Dahlberg, A. E. & Frank, J. (1999). Major rearrangements in the 70S ribosomal 3D structure caused by a conformational switch in 16S ribosomal RNA. *EMBO Journal* **18**, 6501–6507.

Gavrilova, L. P., Kostiashkina, O. E., Koteliansky, V. E., Rutkevitch, N. M. & Spirin, A. S. (1976). Factor-free (non-enzymic) and factor-dependent systems of translation of polyuridylic acid by *Escherichia coli* ribosomes. *Journal of Molecular Biology* **101**, 537–552.

Go, N. (1983). Theoretical-studies of protein folding. *Annual Review of Biophysics and Bioengineering* **12**, 183–210.

Hamacher, K., Trylska, J. & McCammon, J. A. (2006). Dependency map of proteins in the small ribosomal subunit. *Plos Computational Biology* **2**, 80–87.

Harms, J., Schluenzen, F., Zarivach, R., Bashan, A., Gat, S., Agmon, I., Bartels, H., Franceschi, F. & Yonath, A. (2001). High resolution structure of the large ribosomal subunit from a mesophilic Eubacterium. *Cell* **107**, 679–688.

Held, W. A., Ballou, B., Mizushim, S. & Nomura, M. (1974). Assembly mapping of 30 S ribosomal-proteins from *Escherichia coli* – further studies. *Journal of Biological Chemistry* **249**, 3103–3111.

Hermann, T. (2005). Drugs targeting the ribosome. *Current Opinion in Structural Biology* **15**, 355–366.

Honig, B. & Nicholls, A. (1995). Classical electrostatics in biology and chemistry. *Science* **268**, 1144–1149.

Humphrey, W., Dalke, A. & Schulten, K. (1996). VMD: visual molecular dynamics. *Journal of Molecular Graphics* **14**, 33–38.

Ishida, H. & Hayward, S. (2008). Path of nascent polypeptide in exit tunnel revealed by molecular dynamics simulation of ribosome. *Biophysical Journal* **95**, 5962–5973.

Jenni, S. & Ban, N. (2003). The chemistry of protein synthesis and voyage through the ribosomal tunnel. *Current Opinion in Structural Biology* **13**, 212–219.

Kirmizialtin, S., Ganesan, V. & Makarov, D. E. (2004). Translocation of a beta-hairpin-forming peptide through a cylindrical tunnel. *Journal of Chemical Physics* **121**, 10268–10277.

Klein, D. J., Moore, P. B. & Steitz, T. A. (2004). The roles of ribosomal proteins in the structure assembly, and evolution of the large ribosomal subunit. *Journal of Molecular Biology* **340**, 141–177.

Korostelev, A., Ermolenko, D. N. & Noller, H. F. (2008). Structural dynamics of the ribosome. *Current Opinion in Chemical Biology* **12**, 674–683.

Kurkcuoglu, O., Doruker, P., Sen, T. Z., Kloczkowski, A. & Jernigan, R. L. (2008). The ribosome structure controls and directs mRNA entry, translocation and exit dynamics. *Physical Biology* **5**, 46005.

Kurkcuoglu, O., Kurkcuoglu, Z., Doruker, P. & Jernigan, R. L. (2009). Collective dynamics of the ribosomal tunnel revealed by elastic network modeling. *Proteins* **75**, 837–845.

Liljas, A. (2004). *Structural Aspects of Protein Synthesis*. Singapore: World Scientific Publishing Co. Pte. Ltd.

Lu, J. L. & Deutsch, C. (2005). Folding zones inside the ribosomal exit tunnel. *Nature Structural & Molecular Biology* **12**, 1123–1129.

Ma, C. S., Baker, N. A., Joseph, S. & Mccammon, J. A. (2002). Binding of aminoglycoside antibiotics to the small ribosomal subunit: a continuum electrostatics investigation. *Journal of the American Chemical Society* **124**, 1438–1442.

Malhotra, A., Tan, R. K. Z. & Harvey, S. C. (1994). Modeling large RNAs and ribonucleoprotein-particles using molecular mechanics techniques. *Biophysical Journal* **66**, 1777–1795.

Meroueh, S. O. & Mobashery, S. (2007). Conformational transition in the aminoacyl t-RNA site of the bacterial ribosome both in the presence and absence of an aminoglycoside antibiotic. *Chemical Biology & Drug Design* **69**, 291–297.

Mitra, K., Schaffitzel, C., Fabiola, F., Chapman, M. S., Ban, N. & Frank, J. (2006). Elongation arrest by SecM via a cascade of ribosomal RNA rearrangements. *Molecular Cell* **22**, 533–543.

Munro, J. B., Vaiana, A., Sanbonmatsu, K. Y. & Blanchard, S. C. (2008). A new view of protein synthesis: mapping the free energy landscape of the

https://doi.org/10.1017/S0033583510000028 Published online by Cambridge University Press

ribosome using single-molecule FRET. *Biopolymers* **89**, 565–577.

NAKATOGAWA, H. & ITO, K. (2002). The ribosomal exit tunnel functions as a discriminating gate. *Cell* **108**, 629–636.

POEHLSGAARD, J. & DOUTHWAITE, S. (2005). The bacterial ribosome as a target for antibiotics. *Nature Reviews Microbiology* **3**, 870–881.

POWERS, T., DAUBRESSE, G. & NOLLER, H. F. (1993). Dynamics of in-vitro assembly of 16-S ribosomal-RNA into 30-S ribosomal-subunits. *Journal of Molecular Biology* **232**, 362–374.

QIN, S. B. & ZHOU, H. X. (2009). Dissection of the high rate constant for the binding of a ribotoxin to the ribosome. *Proceedings of the National Academy of Sciences USA* **106**, 6974–6979.

QIZHI CUI, R. Z-K. TAN, HARVEY, S. C. & CASE, D. A. (2006). Low-resolution molecular dynamics simulations of the 30S ribosomal subunit. *Multiscale Modeling and Simulation* **5**, 1248–1263.

REBLOVA, K., LANKAS, F., RAZGA, F., KRASOVSKA, M. V., KOCA, J. & SPONER, J. (2006). Structure, dynamics, and elasticity of free 16S rRNA helix 44 studied by molecular dynamics simulations. *Biopolymers* **82**, 504–520.

RODNINA, M. V., BERINGER, M. & WINTERMEYER, W. (2006). Mechanism of peptide bond formation on the ribosome. *Quarterly Reviews of Biophysics* **39**, 203–225.

ROMANOWSKA, J., SETNY, P. & TRYLSKA, J. (2008). Molecular dynamics study of the ribosomal A-site. *Journal of Physical Chemistry B* **112**, 15227–15243.

SANBONMATSU, K. Y. (2006). Energy landscape of the ribosomal decoding center. *Biochimie* **88**, 1053–1059.

SANBONMATSU, K. Y., JOSEPH, S. & TUNG, C. S. (2005). Simulating movement of tRNA into the ribosome during decoding. *Proceedings of the National Academy of Sciences USA* **102**, 15854–15859.

SANBONMATSU, K. Y. & TUNG, C. S. (2007). High performance computing in biology: multimillion atom simulations of nanoscale systems. *Journal of Structural Biology* **157**, 470–480.

SCHLICK, T. (2002). *Molecular Modeling and Simulation*, Springer-Verlag.

SCHLUENZEN, F., TOCILJ, A., ZARIVACH, R., HARMS, J., GLUEHMANN, M., JANELL, D., BASHAN, A., BARTELS, H., AGMON, I., FRANCESCHI, F. & YONATH, A. (2000). Structure of functionally activated small ribosomal subunit at 3·3 angstrom resolution. *Cell* **102**, 615–623.

SOUTHWORTH, D. R., BRUNELLE, J. L. & GREEN, R. (2002). EFG-independent translocation of the mRNA: tRNA complex is promoted by modification of the ribosome with thiol-specific reagents. *Journal of Molecular Biology* **324**, 611–623.

STAGG, S. M., MEARS, J. A. & HARVEY, S. C. (2003). A structural model for the assembly of the 30 S subunit of the ribosome. *Journal of Molecular Biology* **328**, 49–61.

TALKINGTON, M. W. T., SIUZDAK, G. & WILLIAMSON, J. R. (2005). An assembly landscape for the 30S ribosomal subunit. *Nature* **438**, 628–632.

TAMA, F., VALLE, M., FRANK, J. & BROOKS, C. L. (2003). Dynamic reorganization of the functionally active ribosome explored by normal mode analysis and cryo-electron microscopy. *Proceedings of the National Academy of Sciences USA* **100**, 9319–9323.

TENSON, T. & EHRENBERG, M. (2002). Regulatory nascent peptides in the ribosomal tunnel. *Cell* **108**, 591–594.

TRYLSKA, J., KONECNY, R., TAMA, F., BROOKS, C. L. & MCCAMMON, J. A. (2004). Ribosome motions modulate electrostatic properties. *Biopolymers* **74**, 423–431.

TRYLSKA, J., MCCAMMON, J. A. & BROOKS, C. L. (2005a). Exploring assembly energetics of the 30S ribosomal subunit using an implicit solvent approach. *Journal of the American Chemical Society* **127**, 11125–11133.

TRYLSKA, J., TOZZINI, V. & MCCAMMON, J. A. (2005b). Exploring global motions and correlations in the ribosome. *Biophysical Journal* **89**, 1455–1463.

TUNG, C. S. & SANBONMATSU, K. Y. (2004). Atomic model of the Thermus thermophilus 70S ribosome developed in silico. *Biophysical Journal* **87**, 2714–2722.

VAIANA, A. C. & SANBONMATSU, K. Y. (2009). Stochastic gating and drug-ribosome interactions. *Journal of Molecular Biology* **386**, 648–661.

VALLE, M., ZAVIALOV, A., SENGUPTA, J., RAWAT, U., EHRENBERG, M. & FRANK, J. (2003). Locking and unlocking of ribosomal motions. *Cell* **114**, 123–134.

VOSS, N. R., GERSTEIN, M., STEITZ, T. A. & MOORE, P. B. (2006). The geometry of the ribosomal polypeptide exit tunnel. *Journal of Molecular Biology* **360**, 893–906.

WANG, Y. M., RADER, A. J., BAHAR, I. & JERNIGAN, R. L. (2004). Global ribosome motions revealed with elastic network model. *Journal of Structural Biology* **147**, 302–314.

WILLIAMSON, J. R. (2008). Biophysical studies of bacterial ribosome assembly. *Current Opinion in Structural Biology* **18**, 299–304.

WILSON, D. N. & NIERHAUS, K. H. (2003). The ribosome through the looking glass. *Angewandte Chemie-International Edition* **42**, 3464–3486.

WIMBERLY, B. T., BRODERSEN, D. E., CLEMONS, W. M., MORGAN-WARREN, R. J., CARTER, A. P., VONRHEIN, C., HARTSCH, T. & RAMAKRISHNAN, V. (2000). Structure of the 30S ribosomal subunit. *Nature* **407**, 327–339.

YAN, A. M., WANG, Y. M., KLOCZKOWSKI, A. & JERNIGAN, R. L. (2008). Effects of protein subunits removal on the computed motions of partial 30S structures of the ribosome. *Journal of Chemical Theory and Computation* **4**, 1757–1767.

YANG, G., TRYLSKA, J., TOR, Y. & MCCAMMON, J. A. (2006). Binding of aminoglycosidic antibiotics to the oligonucleotide A-site model and 30S ribosomal subunit: Poisson–Boltzmann model, thermal denaturation, and fluorescence studies. *Journal of Medicinal Chemistry* **49**, 5478–5490.

https://doi.org/10.1017/S0033583510000028 Published online by Cambridge University Press

Yusupov, M. M., Yusupova, G. Z., Baucom, A., Lieberman, K., Earnest, T. N., Cate, J. H. D. & Noller, H. F. (2001). Crystal structure of the ribosome at 5·5 angstrom resolution. *Science* **292**, 883–896.

Ziv, G., Haran, G. & Thirumalai, D. (2005). Ribosome exit tunnel can entropically stabilize alpha-helices. *Proceedings of the National Academy of Sciences USA* **102**, 18956–18961.

https://doi.org/10.1017/S0033583510000028 Published online by Cambridge University Press